Reaction Dynamics of H_2O^+ (D_2O^+) + NH_3 Studied with Crossed Molecular Beams and Density Functional Theory Calculations†

Yue Li and James M. Farrar*

Department of Chemistry, University of Rochester, Rochester, New York 14627

Received: April 29, 2004; In Final Form: July 12, 2004

The charge transfer and proton transfer reactions between H_2O^+ (D_2O^+) and NH_3 were studied at collision energies below 1 eV using the crossed molecular beam technique and density functional theory (DFT) calculations. The reaction products include NH_3D^+ formed by deuterium ion transfer, NH_3^+ produced by charge transfer, and NH_2D^+ formed by charge transfer with H/D exchange. These three products are formed in the ratio of 1.0:2.0:1.2, respectively. The center of mass flux distributions of the product ions for all three reaction channels exhibit asymmetry, with maxima close to the velocity and direction of the precursor ammonia beam, characteristic of direct reactions. The internal energy distributions of the products of charge transfer are independent of collision energy, are very narrow (∼0.55 eV) and are peaked at the reaction exothermicity of 2.55 eV. The NH_2D^+ products have very similar distributions, peaking at the reaction exothermicity and having widths of ∼0.70 eV. The mechanisms for these reaction channels are discussed on the basis of the DFT calculated potential energy surfaces, which identify three electrostatically bound complexes of the form $[H_2O{\cdot}NH_3]^+$ that mediate reaction. Theory suggests that H/D exchange to form NH_2D^+ may occur through the complex $NH_3D^+{\cdots}OD$, in which an internal rotation of the NH_3D^+ unit exchanges hydrogen and deuterium atoms. The large fraction of NH_2D^+ reaction products observed indicates that this exchange takes place at a rate nearly 3 orders of magnitude faster than the predictions of statistical theory.

I. Introduction

Understanding the microscopic mechanisms of chemical reactions at the level of the forces that approaching reactants and separating products exert on one another is a major goal of chemical kinetics. Charge transfer and proton transfer, considered the simplest chemical reactions, have thus long attracted the interest of theoreticians and experimentalists.[1−9] Water and ammonia are both important small molecules that can form a stable hydrogen-bonded adduct, either as a neutral or ionic complex.[10−19] Chemical reactions between these species or occurring within complexes of these species include electron transfer and particle exchange and therefore provide paradigms for the most elementary reactions in systems amenable to theoretical treatments via ab initio quantum chemistry. In a recent paper,[20] we reported the crossed beam experimental results of the proton transfer reaction between H_3O^+ and NH_3. This reaction is found to proceed through a classic "induced repulsive energy release" mechanism[21,22] to produce highly vibrationally excited NH_4^+ products, with excitation primarily in N−H stretching modes. In this study, we investigated a related system, the charge transfer and proton transfer reactions between H_2O^+ and NH_3, using the crossed molecular beam technique and DFT calculations. The observed ions correspond to the products of the following two reactions.

$$H_2O^+ + NH_3 \rightarrow OH + NH_4^+ \qquad \Delta H = -2.70 \text{ eV } (-260.5 \text{ kJ/mol}) \quad (1)$$

$$\rightarrow H_2O + NH_3^+ \qquad \Delta H = -2.55 \text{ eV } (-246.0 \text{ kJ/mol}) \quad (2)$$

The enthalpy changes of reactions 1 and 2 are determined from tabulated heats of formation of reactants and products.[23]

An early experimental study for this system was conducted by Anicich et al.,[24] who used tandem and trapped ion ICR techniques to measure the rate constants of $H_2{}^{18}O^+ + NH_3$ producing NH_3^+ and NH_4^+. The authors found that the charge transfer and proton transfer products were formed in a 70%: 30% ratio. They also found that the charge transfer rate constant is much larger than predicted by the average dipole orientation (ADO) theory[25] and suggested that some charge transfer outside the orbiting impact parameter range may occur. In related work, Vancura and Herman[26] performed crossed-beam scattering experiments to study the following hydrogen abstraction reaction:

$$D_2O^+ + NH_3 \rightarrow D_2HO^+ + NH_2 \qquad \Delta H = -1.48 \text{ eV } (-142.8 \text{ kJ/mol}) \quad (3)$$

They suggested two mechanisms for the production of D_2HO^+: direct hydrogen atom transfer and decomposition of an intermediate complex, $[D_2O{\cdot}NH_3]^+$. They suggested that the intermediate complex has a structure denoted as $D_2OH^+{\cdots}NH_2$, in which the proton bridge between the heavy atoms has a linear geometry. Theoretically, Sodupe et al.[27] used ab initio calculations to obtain three different structures of the $[H_2O{\cdot}NH_3]^+$ complex and estimates of the relative energies of several probable dissociation channels. However, they did not calculate transition states, and thus could not discuss reaction mechanisms. Three isomers of $[H_2O{\cdot}NH_3]^+$, very similar to those calculated by Sodupe et al., were also obtained by Tachibana et al.[28] at the MP2(full)/6-31G* level. Their results show that a hydrogen-bonded structure in which NH_3 acts as the proton donor is the most stable one. Tachibana et al. also obtained two transition

† Part of the special issue "Tomas Baer Festschrift".

10.1021/jp0481310 CCC: $27.50
Published on Web 08/24/2004

states for specific decomposition channels of the complexes to products. These theoretical results will be discussed in more detail in the paper.

The endothermic reaction between NH_3^+ and H_2O, the charge transferred reactants of the present study, has also been extensively studied. In a tandem and trapped ion ICR study, Anicich et al.[24] found that the reaction rate of internally excited NH_3^+ ions with H_2O is much faster than that of ground state ions, as expected for an endothermic reaction. The NH_3^+ ions in the ground state only form NH_4^+, whereas for NH_3^+ ions in vibrationally excited states, the dominant product ions are the hydrogen atom transfer products, H_3O^+(85%). The distribution of the two products, H_3O^+ and NH_4^+, is found to be strongly dependent on the internal energy of NH_3^+; thus, the above reaction was used to determine the total amount of internal energy deposited in the NH_3^+ ions produced by charge transfer reactions.[29]

A photoionization study of an NH_3 and H_2O gaseous mixture by Chupka and Russell[30] showed that increasing vibrational energy in NH_3^+ had no effect on the reaction cross section of the hydrogen atom transfer reaction $NH_3^+ + H_2O \rightarrow NH_4^+ + OH$. Chesnavich and Bowers[31] performed phase space theory calculations for this system, showing that the reaction cross section decreased by about 90% as the vibrational energy increased from zero to 1.5 eV, a tendency inconsistent with the photoionization results of Chupka and Russell. Therefore, they suggested that the reaction proceeds nonstatistically.

Zare and co-workers[32] studied the reactions of vibrationally state-selected NH_3^+ ions with D_2O using a quadrupole-octopole-quadrupole apparatus at center of mass (c.m.) collision energies between 0.5 and 10.0 eV, with NH_3^+ prepared in the ν_2 umbrella bending mode with zero to 10 quanta, and in a combination mode with one quantum of ν_1 N−H symmetric stretching and two quanta of the ν_2 umbrella bending mode. They found that the predominant product ions are NH_2D^+ (mass 18) and D_2HO^+ (mass 21), resulting from isotope exchange and proton transfer, respectively. Only small amounts of NH_3D^+ (mass 19), $NH_2D_2^+$ (mass 20) and ND_4^+ (mass 22) were observed in their experiments. For the proton transfer products, the cross section of the reaction was found to decrease with increasing collision energy. However, it was also observed that the reaction cross section increases with increasing internal energy of the NH_3^+ ion, but without a specific vibrational-mode selectivity. For the isotope exchange products, they suggested a two-step mechanism: a collision-induced dissociation-mediated complex formation followed by the dissociation of this complex into products. In a related study, Green and Zare[33] studied the reaction of deuterium-substituted reactants $ND_3^+ + D_2O \rightarrow ND_4^+ + OD$. They used REMPI to prepare ND_3^+ and measured the rotational distribution of the OD ($\nu = 0$) product using laser-induced fluorescence. Their results are in excellent agreement with an RRKM type model, leading them to suggest that the reaction proceeds through a long-lived complex.

In the crossed-beam experiments of this study, we measured reactive scattering between H_2O^+ (D_2O^+) and NH_3. In contrast to Vancura and Herman, we observed the products of charge transfer and proton transfer reactions, in addition to NH_2D^+ ions, which result from charge transfer with isotope exchange via

$$D_2O^+ + NH_3 \rightarrow NH_2D^+ + HOD \qquad (4)$$

A comparison of this reaction with direct charge transfer, reaction 2, is particularly instructive: although one can envision the latter reaction proceeding via long-range electron transfer, the isotope exchange process occurring in reaction 4 must clearly involve regions of the potential energy surface where the nuclei are in close proximity. To assist us in the interpretation of the results, we also performed the DFT calculations to assess the roles of various intermediate complexes occurring between reactants and products.

II. Experimental Section

The experimental apparatus is as described in previous publications.[20] The H_2O^+ (D_2O^+) ions were produced by electron impact on a room temperature gaseous water (or deuterium oxide, 99.9%, Cambridge Isotope Laboratories, Inc.) and hydrogen mixture. The pressure in the ion source is typically 10^{-2} Torr. The ions are mass-selected with a 60° magnetic sector. After deceleration to the desired beam energy, the ion beam has an energy distribution with fwhm of 0.25 to 0.40 eV. The neutral beam was formed by supersonic expansion of the pure ammonia gas through a 0.07 mm nozzle. A 1.0 mm diameter skimmer, located 50 nozzle diameters downstream from the nozzle, selects the cool core of the beam. The beam enters a differential pumping chamber, where it is collimated with a 3.0 mm square aperture located approximately 2.5 cm from the skimmer, before entering the main chamber, where it intersects with the ion beam at a 90° angle. A tuning fork chopper modulates the beam at 30 Hz to provide the time synchronization for the experiment. A rotatable electrostatic energy analyzer with a laboratory resolution of 0.07 eV was used to measure the kinetic energies of the reactant and product ions. The product ions were mass-analyzed with a quadrupole mass spectrometer and detected with a dual microchannel plate ion detector. Data were collected with a computer-controlled multichannel scalar synchronized with the beam modulation. The energy analyzer was calibrated before and after the experiments. The resonant charge transfer reaction between He^+ and He was used as the calibration reaction to determine the zero offset of the energy analyzer.

Two independent measurements were performed in the experiment. The kinetic energy distributions of the scattered product ions were measured at 15 to 20 fixed laboratory angles. Each energy spectrum consisted of 80 points, with typical energy bin widths of 0.025 eV. These kinetic energy distributions were then normalized by measuring angular distributions of product ions in the laboratory coordinate system by summing the signal over all energies. In addition, the branching ratios for the products of all three reactive channels were determined at each collision energy.

III. Data Analysis

The experimental intensities for reactions (1), (2), and (4) were transformed to the c.m. coordinate system. The reactant beams in the experiments have velocity and angular spreads, resulting in distributions of collision energies and intersection angles. These dispersions must be taken into account when transforming the laboratory data to c.m. coordinates. An iterative deconvolution procedure is used to extract the c.m. cross section from the laboratory flux distributions by inverting the following equation:[34]

$$I_{\mathrm{lab}}(v,\Theta) = \sum_{i=1}^{N} f_i \frac{v^2}{u_i^2} I_{\mathrm{c.m.}}(u_i,\theta_i) \qquad (5)$$

In eq 5, v and u_i are the velocities in the laboratory and c.m. coordinates, respectively, and f_i is the weighing factor, or the probability of observing Newton diagram i based on the reagent

beam distributions. Five points are used to represent the energy distributions of each of the two reagent beams, and five points represent the intersection angle distribution; thus, in the above equation, N is 125. Application of this deconvolution procedure produces c.m. cross sections $I_{c.m.}(u, \theta)$, that when transformed back to laboratory with appropriate averaging over experimental velocity distributions and beam intersection angles, recover the experimental data with a standard deviation of < 10%.

The barycentric angular distributions $g(\theta)$ of the products, representing the relative intensities of products scattered into c.m. scattering angle θ averaged over product kinetic energy, are calculated by integration over c.m. speed u, as indicated in

$$g(\theta) = \int_0^\infty I_{c.m.}(u,\theta)\, du \qquad (6)$$

Similarly, the angle-averaged relative translational energy distribution of products, $P(E_T')$, are calculated by integrating the c.m. intensity over angle, as follows:

$$P(E_T') = \int_0^\pi u^{-1} I_{c.m.}(u,\theta) \sin\theta\, d\theta \qquad (7)$$

The full flux distributions in velocity space as well as the kinetic energy and angular distributions derived from them provide important physical insight into the nature of reactive collisions.

IV. Experimental Results

A. Deuterium Cation Transfer Reaction $D_2O^+ + NH_3 \rightarrow OD + NH_3D^+$. The proton transfer reaction 1 forms products of mass 18, which cannot be distinguished from nonreactively scattered H_2O^+. Consequently, we used D_2O^+ to study the production of NH_3D^+ by deuterium ion transfer. The reaction was studied at c.m. collision energies of 0.51, 0.74 and 1.02 eV (49.2, 71.4 and 98.4 kJ/mol), respectively. Three kinds of product ions were observed: NH_3^+ (mass 17), NH_2D^+ (mass 18) and NH_3D^+ (mass 19). The D_2HO^+ ions (mass 21), products of hydrogen atom transfer, have been measured by Vancura and Herman[26] using the crossed-beam scattering technique, as discussed in the Introduction section. However, we did not observe product ions with mass number 21 or higher.

Figure 1 shows the product ion polar flux contour map for NH_3D^+ products formed by D^+ transfer at a collision energy of 1.02 eV (98.4 kJ/mol). In the figure, 0° is defined as the direction of the reactant ion beam in c.m. coordinates, whereas 180° defines the direction of the neutral beam. At all three experimental collision energies, the flux distributions are asymmetric and the distribution peaks are close to the velocity and direction of the precursor ammonia beam. Such flux distributions are the signature of a direct reaction, resulting in little change of momentum of the NH_3 unit after D^+ transfer. Any intermediate complex in the reaction must be short-lived; if the lifetime of any such species were at least a rotational period, the scattered ion distributions would have a significant backward scattered component that would lead to a distribution symmetric with respect to the backward and forward directions in c.m. coordinates at very low collision energies.

The angular distributions and relative translational energy distributions of the products NH_3D^+ obtained from equations (6) and (7) are shown in Figure 2. The relative translational energy distributions of the products shift toward higher energies and broaden slightly with increasing collision energy. The product average translational energies at the three collision energies increase from 24% to 30% of the total available energy over this collision energy range.

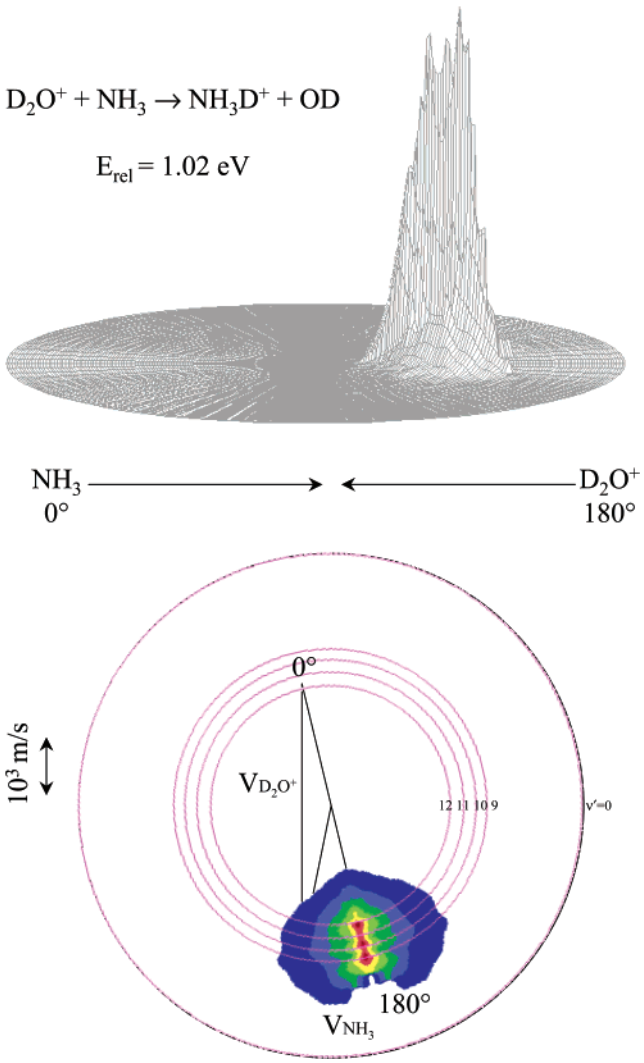

Figure 1. Newton diagram and scattered product contour map of the deuterium cation transfer reaction $D_2O^+ + NH_3 \rightarrow OD + NH_3D^+$ at the relative energy of 1.02 eV. Concentric circles on the contour map denote loci of points corresponding to formation of NH_3D^+ with specified number of quanta in ν_2 N−D stretching mode coincident with ground state OD. The circle labeled $\nu' = 0$ defines the maximum velocity of NH_3D^+ products allowed by energy conservation.

The deuterium cation transfer involves a fast motion of the D^+ ion from oxygen to nitrogen as the new N−D bond is formed. Such light atom transfer is generally described by "mixed energy release",[35−38] in which both the cleaving and nascent bonds are extended from their equilibrium displacements. One can expect that the transfer will result in significant stretching excitation of the nascent N−D bond. For NH_3D^+, the vibration corresponding to N−D stretching is the nondegenerate ν_2 mode at 2430.8 cm^{-1}.[39] We attempt to use the ν_2 mode frequency with anharmonic corrections to calculate the vibrational energy levels of the products. The region in the vicinity of maximum flux in the contour map shows a structure composed of three peaks of comparable intensity. These peaks fall on the circles corresponding to formation of NH_3D^+ products with specific numbers of quanta in the ν_2 N−D stretching mode. In Figure 2(b), the corresponding vibrational band structures assigned to vibrational quantum number of 12, 11, 10, and 9 can also be observed in the product translational energy distributions, but because of the angular averaging inherent in the calculation of the kinetic energy distribution, in eq 5, the structure is washed out. In addition to the effect of angular

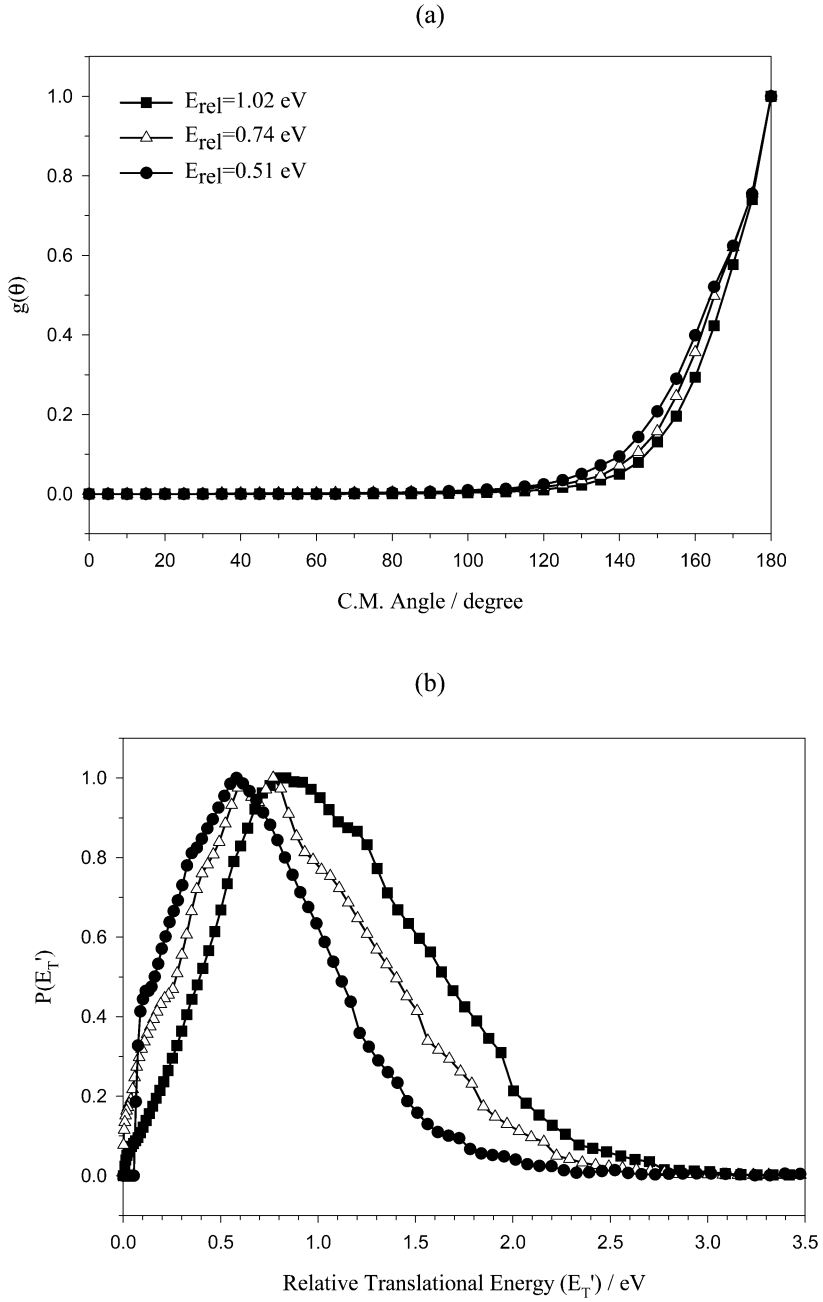

Figure 2. (a) Angular distributions in c.m. coordinates. (b) Relative translational energy distributions of the product NH_3D^+ ions at three relative energies.

averaging, this washing out of structure may also be a consequence of excitation of other vibrations, or of rotational excitation in the OD fragment.

B. Charge Transfer Reaction $H_2O^+ + NH_3 \rightarrow H_2O + NH_3^+$. Measurements for the reaction of H_2O^+ with NH_3 were performed at selected c.m. collision energies of 0.37, 0.66, and 0.94 eV (35.7, 63.7, and 90.7 kJ/mol respectively). The c.m. polar flux representation of the experimental data for NH_3^+ formed by charge transfer at a collision energy of 0.66 eV (63.7 kJ/mol), obtained by deconvolution as described in the previous section is shown in Figure 3. The flux distributions for the other two collision energies are similar to Figure 3 and are not reported here. The angular distributions and relative translational energy distributions of the charge transfer products at all three collision energies are shown in Figure 4.

It is evident from Figure 3 and Figure 4(a) that at all collision energies, the product ion flux distributions are asymmetric and the maxima are at 180° in c.m. coordinates. This observation indicates that the NH_3^+ ion has nearly the same direction as the precursor NH_3 beam, and corresponds to forward scattering. Thus, the charge transfer reaction is direct. The reaction takes place through large impact parameters, resulting in little change of momentum of the NH_3 unit during the charge transfer process.

The energy partitioning results for NH_3^+ formed by charge transfer are listed in Table 1. The data of Table 1 and the product kinetic energy distributions of Figure 4(b) show that as the collision energy is increased, the average relative translational energy of the products increases. With increasing collision energy, the fraction of the total energy available to the products increases from 17% to 27%.

C. H/D Exchange Reaction $D_2O^+ + NH_3 \rightarrow HDO + NH_2D^+$. We also observed products at mass 18, corresponding to the formation of NH_2D^+. In their study of the $NH_3^+ + D_2O$ reaction, Zare and co-workers[32] also observed NH_2D^+ ions, and they suggested that NH_2D^+ is formed by a two-step mechanism in which collision-induced dissociation of the NH_3^+ ion results

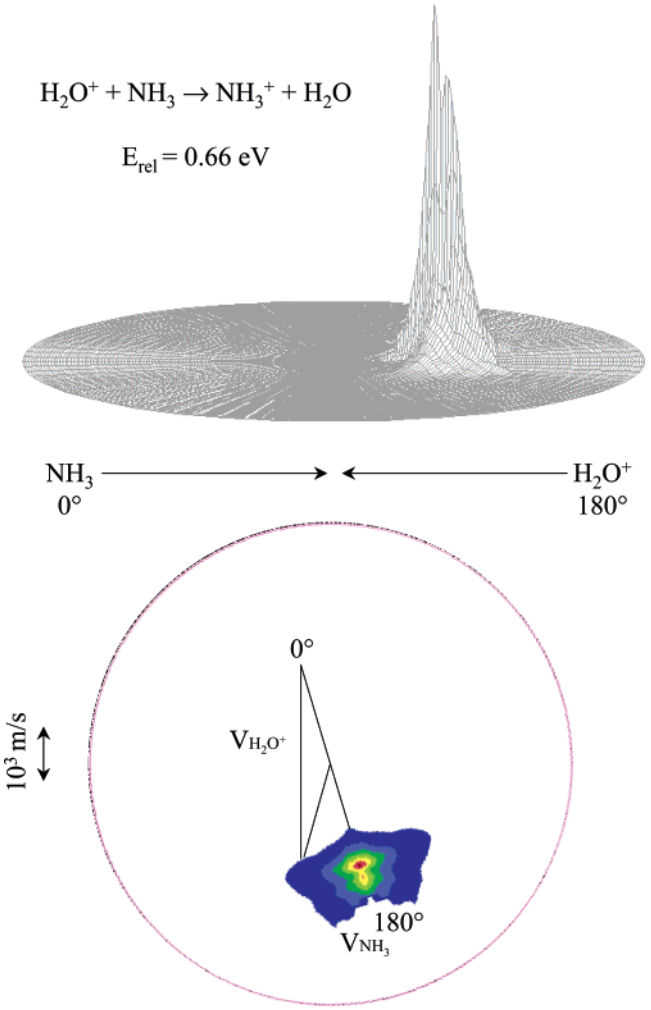

Figure 3. Newton diagram and scattered product contour map of the charge transfer reaction $H_2O^+ + NH_3 \rightarrow H_2O + NH_3^+$ at the relative energy of 0.66 eV. The circle on the contour map defines maximum NH_3^+ product velocity allowed by energy conservation.

TABLE 1: Reaction Energy Partitioning Results (eV)

$D_2O^+ + NH_3 \rightarrow NH_3D^+ + OD$			
collision energy, E_{rel}	0.51	0.74	1.02
total energy, E_{total}	3.21	3.44	3.72
product average relative energy, E_T'	0.77	0.93	1.11
E_T'/E_{total}	24%	27%	30%
product average internal energy	2.44	2.51	2.61
$H_2O^+ + NH_3 \rightarrow NH_3^+ + H_2O$			
collision energy, E_{rel}	0.37	0.66	0.94
total energy, E_{total}	2.92	3.21	3.49
product average relative energy, E_T'	0.50	0.76	0.95
E_T'/E_{total}	17%	24%	27%
product average internal energy	2.42	2.45	2.54
$D_2O^+ + NH_3 \rightarrow NH_2D^+ + HDO$			
collision energy, E_{rel}	0.53	0.69	0.97
total energy, E_{total}	3.08	3.24	3.52
product average relative energy, E_T'	0.67	0.77	0.94
E_T'/E_{total}	22%	24%	27%
product average internal energy	2.41	2.47	2.58

in an intermediate complex $[D_2O{\cdot}NH_2]^+$ and a hydrogen atom. The complex then decays to form $NH_2D^+ + OD$. The collision energies of the present experiments, 0.53, 0.69, and 0.97 eV (51.1, 66.6, and 93.6 kJ/mol, respectively), are well below the thresholds for collisional dissociation of the reactants or of unimolecular decay of nascent NH_3D^+ products to NH_2D^+. In the present study, the signal levels, and the energy and angular distributions of NH_2D^+ are remarkably similar to those of NH_3^+ formed by charge transfer, suggesting that NH_2D^+ formation involves isotope exchange during the process of charge transfer. As shown in Figures 5 and 6a, the flux distributions of the NH_2D^+ ions are asymmetric, with maxima near precursor ammonia beam, and closely resemble the distributions of NH_3^+ formed by direct charge transfer. According to Figure 6 (b), the average product translational energies increase from 0.67 to 0.94 eV, or 22% to 27%, respectively, of the total available energy, over the collision energy range of these experiments. Thus, like the charge transfer and deuterium cation transfer reactions, the total energy is mainly partitioned in the internal energy of the products.

The strongest argument supporting the dynamical relationship between the formation of products NH_3^+ and NH_2D^+ comes from examining the internal energy distributions of the reaction products. These distributions can be obtained from the total energy accessible to the system and the distributions of product translational energy from the following relation:

$$P_{internal}(E') = P_{trans}(E_{total} - E') \quad (8)$$

In the top panel of Figure 7, we plot the internal energy distributions for NH_3^+ formation. Although the experimental data only reveal total internal excitation in all reaction products, not how the energy is partitioned between NH_3^+ and D_2O, it is known that NH_3 undergoes a large geometry change during ionization, from pyramidal to planar.[40] Thus, one expects that the charge transfer process will mainly result in the excitation of the ν_2 umbrella bending mode of NH_3^+. The geometric similarity of D_2O^+ and D_2O suggests that little energy is imparted to this product. Figure 7 (a) shows clearly that the NH_3^+ internal energy distributions are essentially identical at all three collision energies. The widths of the distributions are all approximately 0.55 eV, and all distributions peak sharply at 2.55 eV, the reaction exothermicity. Figure 7 (b) shows the internal energy distributions for NH_2D^+ formation. The similarity with the distributions in NH_3^+ is striking: a sharp peak occurs precisely at the reaction exothermicity and the distributions are essentially energy-independent. The fwhm widths of these distributions are approximately 0.70 eV, an increase of 30% over the widths for charge transfer without isotope exchange.

D. Product Branching Ratios. The use of the isotopically labelled reactant D_2O^+ allows us to distinguish the process of charge transfer to form NH_3^+ from the rearrangement process to form NH_2D^+, in which electron transfer and particle exchange occur together. In the present experiments, we found that the product branching was independent of collision energy. We found that at each collision energy, approximately 75% of the reaction products are formed by charge transfer, yielding either NH_3^+ or NH_2D^+. This result is in good agreement with the 70% value reported in the thermal energy experiments of Anicich et al.[24] It is especially interesting to note that the NH_2D^+ product, which requires that H/D exchange accompany electron transfer, accounts for 37% of all products formed by charge transfer. This fact will be particularly important in evaluating the reaction pathways determined by DFT calculations in the next section of this paper.

V. DFT Calculations

We performed the DFT calculations with the Gaussian-98 program package[41] to elucidate important features of the potential energy surfaces that govern these reactive processes. The geometrical parameters of all neutral and ionic species were

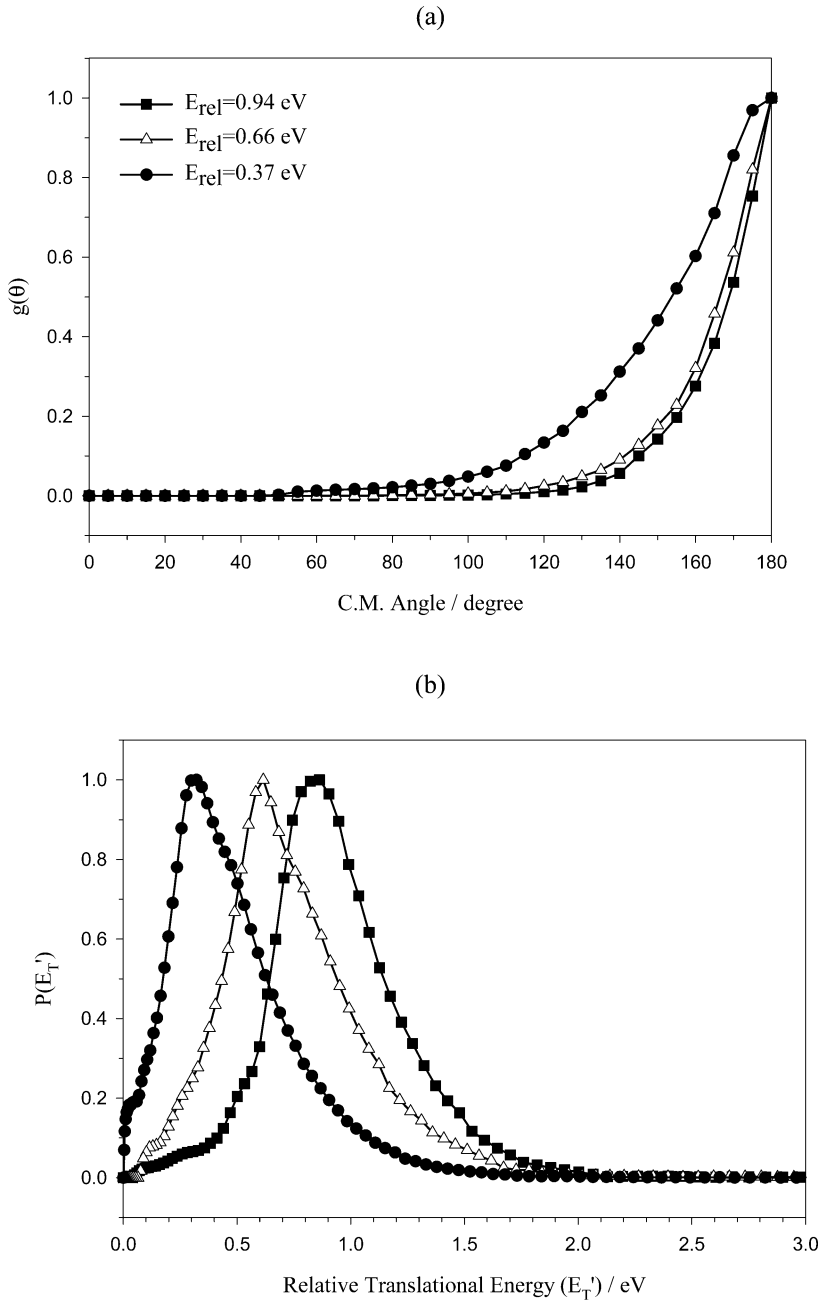

Figure 4. (a) Angular distribution in c.m. coordinates. (b) Relative translational energy distributions of the product NH_3^+ ions at three collision energies.

fully optimized at the DFT(B3LYP) level using the 6-311+G-(d) basis set. The transition states were obtained using the synchronous transit-guided quasi-Newton (STQN) method.[42,43] The stationary points and the first-order saddle points were confirmed through the calculation of harmonic vibrational frequencies. The frequencies of the deuterated species were calculated by replacing the appropriate hydrogen atoms with deuterium. These frequencies were used in the rate constant calculations discussed later. Single point energy calculations based on the B3LYP/6-311+G(d) equilibrium structures were performed at the B3LYP level using the 6-311++G(d,p) basis set. For all open shell species, the expectation values of S^2 are close to 0.75, indicating that spin contamination may be ignored. The geometrical parameters, electronic energies, and vibrational frequencies for all complexes and transition states obtained in this study are listed in the Supporting Information of this paper.

Three isomers for the $[H_2O{\cdot}NH_3]^+$ complex were obtained; a diagram indicating the relative energies of these isomers and their relationships to the reaction products is shown in Figure 8, illustrated with D_2O^+ reactants. The first isomer, denoted **1**, is a hydrogen-bonded complex of nominal structure $NH_4^+\cdots$ OH, in which H_2O acts as the hydrogen donor. Isomer **2** is also hydrogen bonded, but with NH_3 serving as the hydrogen donor. In complex **3**, H_2O and NH_3 are electrostatically bound through an N···O interaction. Three similar structures have been obtained in the MP2 calculations reported in the literature.[27,28] Structure **1** reported here is in good agreement with the MP2 results. However, the DFT calculations of this study show that in isomer **2**, the H_2O and NH_3 units are nearly in a plane (only tilted by 10°) whereas the MP2 calculations predict that the two unit planes are almost perpendicular to each other. At the Hartree−Fock level of theory, we also obtained a perpendicular structure, but at the DFT level, frequency analysis shows that the structure is a transition state, with the imaginary frequency corresponding to an internal rotational of the H_3O unit relative to NH_2. For isomer **3**, the N−O bond length obtained here is 2.23 Å, about

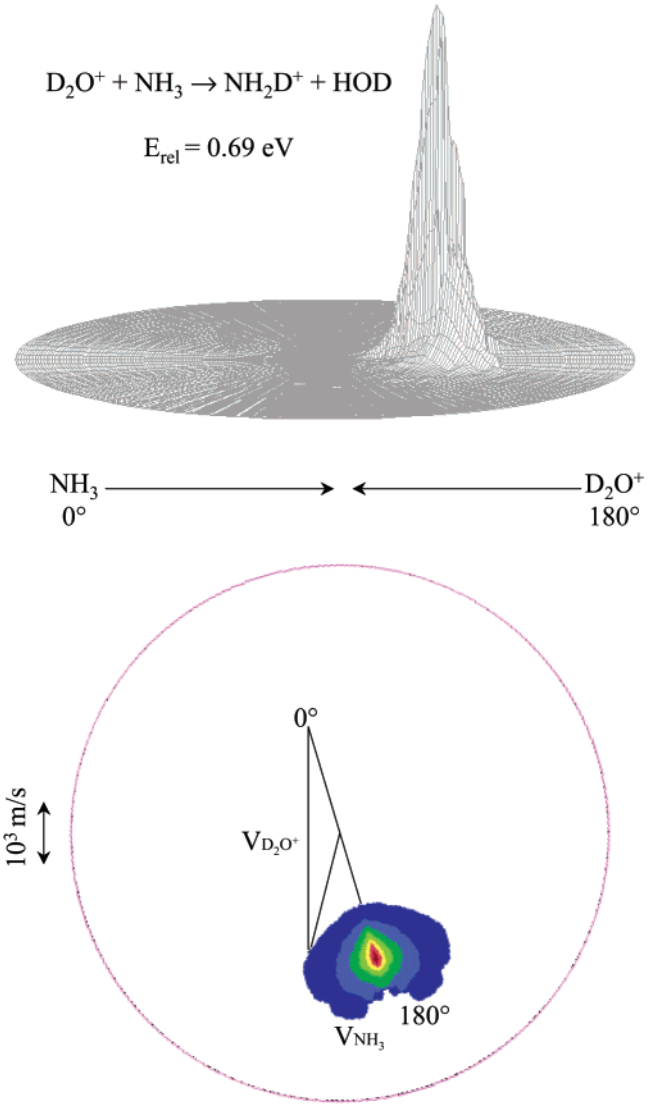

Figure 5. Newton diagram and scattered product contour map of the charge transfer/isotope exchange reaction $D_2O^+ + NH_3 \rightarrow HDO + NH_2D^+$ at the relative energy of 0.69 eV. The circle on the contour map defines maximum NH_2D^+ product velocity allowed by energy conservation.

0.14 Å shorter than the MP2 results. This difference reflects the stronger N−O bond strength calculated by the DFT method, which shows that **3** is slightly more stable than **1**. In contrast, the MP2 calculations predict that the energy of **3** is about 20 kJ/mol higher than that of **1**. In this study, the calculation using the smaller 6-311+G(d) basis set shows that the energy of **3** is 8 kJ/mol higher than **1**. However, using larger basis sets reverses the energy ordering of **1** and **3**. All the calculations predict that isomer **2** is the most stable structure.

Hydrogen atom migration and H/D atom interchange processes play a significant role in the reactive channels in this study, calling attention to the transition states connecting the structures **1**, **2** and **3**. Transformation from **1** to **3** corresponds to a motion of hydrogen in the hydrogen bond from nitrogen to oxygen, and the transition state, $\mathbf{TS_{13}}$, lies 72 kJ/mol above structure **1**. The transition from isomer **2** to **3** requires an internal rotation of the NH_3 unit, which has a low energy barrier, calculated to have an energy of only 18 kJ/mol relative to **2**. The calculations did not produce evidence for a transition state directly connecting **1** and **2**: all attempts to calculate $\mathbf{TS_{12}}$ collapse to $\mathbf{TS_{13}}$. This study also found that the transition state $\mathbf{TS_{11}}$ corresponding to internal rotation of the NH_4^+ unit of isomer **1** lies 13 kJ/mol above structure **1**. On the basis of the error estimates arising from calculation of the exothermicities of reactions 1 and 2, the absolute error limits of these calculations were estimated to be ±10 kJ/mol.

The MP2 study by Tachibana et al.[28] obtained two transition states, but without a clear assignment of which potential wells they connect. According to the calculations reported here, we identify their transition state **TS(HX)** with $\mathbf{TS_{22}}$ of this study, the transition state for an internal rotation of the H_3O unit. Our calculations did not find the transition state they denoted **TS-(HA)**, which they claimed lay 140 kJ/mol above complex **1** and led to either complex **2** or **3**.

In the case of direct charge transfer to form NH_3^+, Figure 8 shows that isomers **1**−**3** are all probable precursors for NH_3^+. Because the charge transfer process involves electron transfer from a nonbonding atomic orbital on the nitrogen atom of NH_3 to the oxygen atom of D_2O^+, we show product formation as originating from complex **3**. To assess the role that the complexes play in the charge transfer process, a calculation of the statistical rate constant for decay of complex **3** to the products of direct charge transfer was performed. The DFT-determined energies and vibrational frequencies for the complex and the loose transition state connecting it to products were used as input parameters for an estimate of the rate constant via the statistical Rice-Ramsperger-Kassel-Marcus (RRKM) theory formula.[44−47] We approximated the transition state frequencies by calculating the frequencies of the $[H_2O{\cdot}NH_3]^+$ structure with the cleaving $(H_2N)H-O(H_2)$ bond extended to 4.5 Å. These frequencies led to an estimate of the activation entropy of the dissociation reactions, $\Delta S^{\ddagger}_{600K}$, for the process (**3** → NH_3^+) of 42 J/(mol·K). The rates of decay for complex **3** to products are approximately 3.5×10^{14} s^{-1}. This rate corresponds to a lifetime for complex **3** of 3 fs, 3 orders of magnitude shorter than the rotational period of the complex estimated from moments of inertia extracted from the DFT calculations. The observation that the dynamics of charge transfer are direct is consistent with this calculation.

A similar analysis holds for the NH_3D^+ products of deuterium ion transfer. The calculations show that complex **1** is the only probable precursor for the formation of this product. Complex **1** dissociates to the NH_3D^+ product over a barrier of 52 kJ/mol, as shown in Figure 8. The DFT calculations show that the entropy of activation for this process is 25 J/(mol·K), indicative of a loose transition state. The resultant RRKM rate constants for product formation are of magnitude 1.5×10^{14} s^{-1} and are also consistent with the direct dynamics we observe for this channel.

Rearrangement charge transfer is the most complex of the reactive processes, requiring H/D exchange, and therefore the participation of one or more intermediate species in which the exchange is facile. The calculations suggest two different pathways for NH_2D^+ formation. The first pathway involves isomerization within intermediate complex **1**, $DO\cdots DNH_3^+$. In this case, internal rotation of the NH_3D^+ unit in **1** exchanges the bridging hydrogen atom through $\mathbf{TS_{11}}$, lying 13 kJ/mol above the energy of **1**. The second pathway proceeds through intermediate complex **2**, $D_2O\cdots HNH_2^+$, in which an internal rotation of the D_2HO^+ unit to form $DHO\cdots DNH_2^+$ precedes decay to products. The relative energy of $\mathbf{TS_{22}}$ is 86 kJ/mol, about 70 kJ/mol higher than $\mathbf{TS_{11}}$. The difference in the energies of these two transition states is consistent with the fact that in $\mathbf{TS_{11}}$, internal rotation disrupts a hydrogen bond, whereas in $\mathbf{TS_{22}}$, a covalent bond must be broken and reformed.

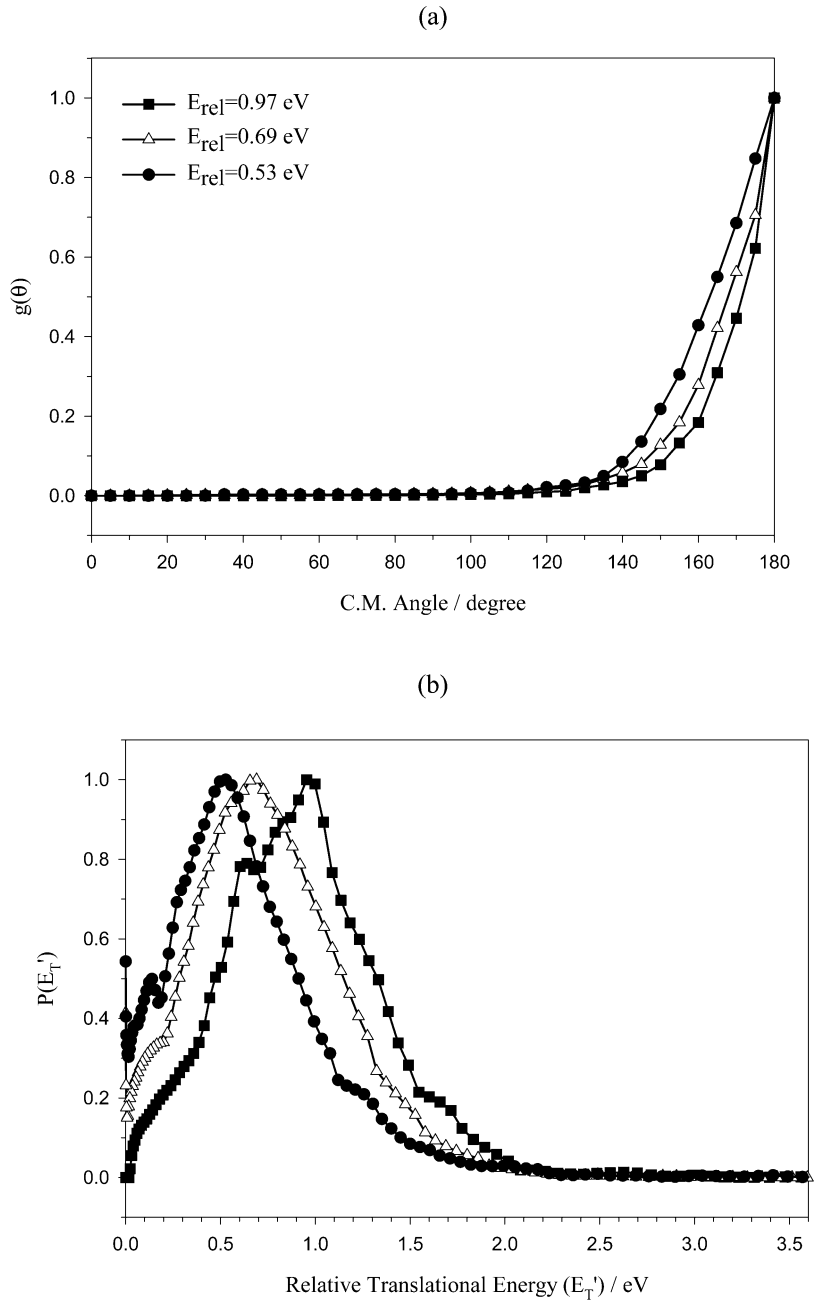

Figure 6. (a) Angular distributions in c.m. coordinates. (b) relative translational energy distributions of the product NH_2D^+ ions at three collision energies.

Statistical rate calculations for the isomerization processes implicated in the H/D exchange processes produce results qualitatively different from those for direct dissociation of intermediates to products. The DFT calculations reveal that the entropies of activation for the rearrangement reactions from **1** to **1′** and **2** to **2′** are −30 and −22 J/(mol·K), respectively, indicative of "tight" transition states. The RRKM rate for **1** to **1′** isomerization is 5×10^{11} s^{-1}, 3 orders of magnitude lower than the direct dissociation of **1′**. The corresponding rearrangement rate from **2** to **2′** is a factor of 5 slower. The statistical rate constants predict that isomerization should be a bottleneck for H/D exchange, resulting in a cross section for NH_2D^+ formation 3 orders of magnitude smaller than for direct charge transfer. This prediction is in clear disagreement with the observation that the cross section for charge transfer with rearrangement is only a factor of 2 smaller than that for direct charge transfer. It is clear that a statistical picture of this process is inappropriate.

VI. Discussion

Although the DFT calculations indicate that reactive trajectories may access the electrostatically bound complexes **1**, **2**, or **3**, the experimental data show that chemical reaction occurs on time scales much faster than the rotational periods of any of these intermediate complexes. The deuterium ion transfer process to form NH_3D^+ exhibits many of the characteristics of direct proton transfer that we have been observed in previous systems.[48−50] In strongly exothermic proton transfer systems, the dynamics appear to be direct, partitioning the majority of the total energy into product vibration. As examples of the heavy + light−heavy mass combination in which the light particle is transferred in reaction, such systems exhibit the energy transfer motif of "mixed energy release",[35−38] in which the reaction occurs with the cleaving and incipient bonds in an extended configuration. This pattern for energy transfer is characteristic of "corner cutting" trajectories on scaled and skewed potential

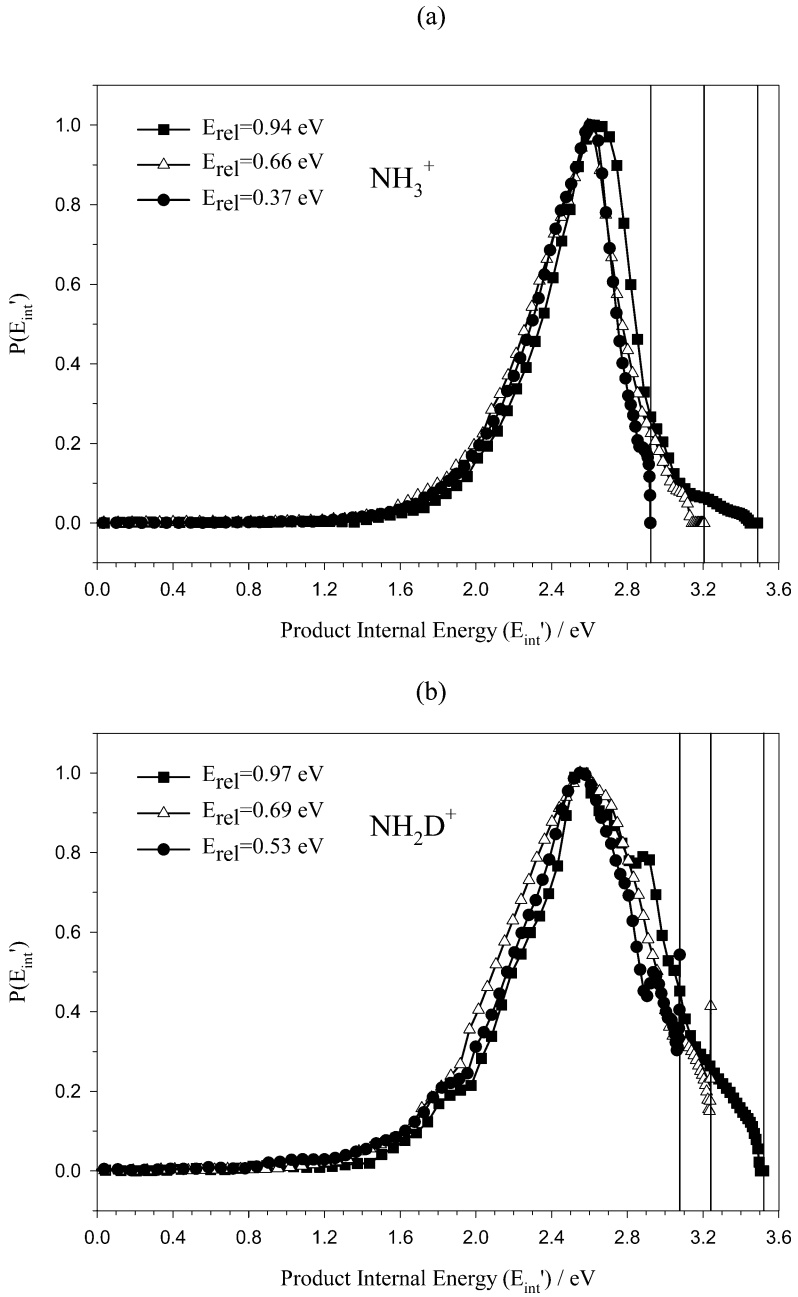

Figure 7. (a) Internal energy distributions of the NH_3^+ products shown at three collision energies. (b) Internal energy distribution of the NH_2D^+ products shown at three collision energies. The solid vertical lines in both panels correspond to the total energies accessible to products.

energy surfaces[51] in which the entrance and exit channels make a small angle with respect to one another and is therefore an intrinsic property of the potential energy surface.

Potential surfaces characteristic of this mass combination also exhibit dynamical features at higher levels of reactant excitation that depend specifically on the nature of the molecular motions excited. Enhanced translational energy can induce trajectories to sample the short-range repulsion in the "corner" of the potential surface, causing particle transfer to occur in geometries in which the breaking and forming bonds are compressed. The effect of such translational excitation in the reactants is to produce incremental product translational and rotational energy, the latter a consequence of sampling bent configurations in the surface corner.[21,22] We observed such "induced repulsive energy release" in our recent study of the $H_3O^+ + NH_3$ proton transfer system.[20] At the lowest collision energy of 0.41 eV, nearly 80% of the total energy of the reaction is partitioned in the internal excitation of the NH_4^+ product ions. However, in the two higher energy experiments, more than 90% of the incremental translational energy appears in relative translational energy of the products. The reaction provides a classic example of the "induced repulsive energy release".

The situation is more subtle in the present case. In the D^+ transfer reaction between D_2O^+ and NH_3, at the lowest collision energy of 0.51 eV, 76% of the total energy appears in product internal excitation, as expected for mixed energy release. At the intermediate collision energy of 0.74 eV, 70% of the incremental translational energy appears in product translation; at the highest collision energy of 1.02 eV, a slightly smaller fraction, 67%, of the increment appears in product translation. Although the reactants in the highest collision energy experiment should be capable of reaching even more compressed configurations with higher repulsive energy, simple conversion of reactant translation into product translation is not operative. One explanation for this unusual observation of a decrease in the incremental translation of the products may arise from the

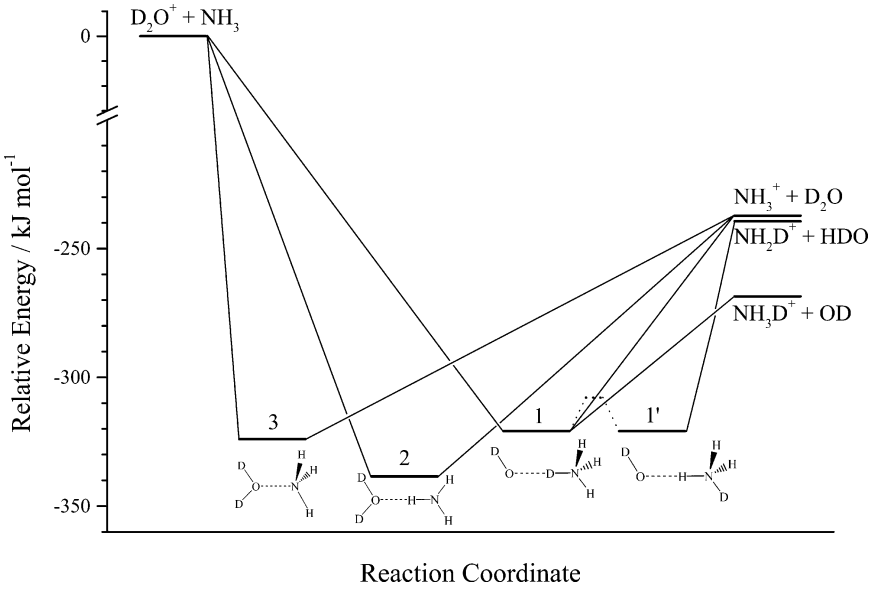

Figure 8. Schematic energy diagram obtained from DFT calculations for NH_3^+, NH_3D^+, and NH_2D^+ formation. Major channels for product formation by direct decay of intermediates are indicated. Dashed lines indicate isomerization pathways and transition states, as discussed in the text.

possibility that in this system, bent configurations become increasingly important at higher collision energies, leading to additional rotational excitation in the fragments.

Another factor that may complicate the simple induced repulsive energy release picture is the potential surface topology associated with the deuterium ion transfer process. To probe this issue, we carried out calculations of the potential energy curves for proton transfer through intermediate **1** at the B3LYP/6-31G(d) level. Distances between oxygen and nitrogen were fixed at three values: 2.8 Å, corresponding to the equilibrium N−O bond length in **1**, 3.1 Å, and 3.4 Å. The O−H bond length was scanned from 0.9 to 2.1 Å in steps of 0.1 Å while other geometrical parameters were optimized. The calculation showed that two potential wells exist, corresponding to structures $[HOH\cdot\cdot\cdot NH_3]^+$ and $[HO\cdot\cdot\cdot HNH_3]^+$, respectively. At the N−O distance of 3.4 Å, the energy barrier connecting the two potential wells is about 1.8 eV relative to the $[HOH\cdot\cdot\cdot NH_3]^+$ structure. As the N−O distance decreases, the energy barrier height lowers. The two-well proton transfer potential energy curves are similar to those obtained for several ionic binary hydrogen-bonded cluster systems.[7,52,53] The double minimum character of the potential surface for proton or deuterium ion transfer may lead to trajectories more complex than those that illustrate the simple concept of induced repulsive energy release.

The experimental data also provide significant insight into the process of charge transfer. In the case of charge transfer to form NH_3^+, direct processes in which electron transfer occurs without significant momentum transfer among all particles are easy to visualize. It is more difficult to visualize H/D exchange in encounters that do not show evidence for the participation of a transient complex. However, it should be recognized that H/D exchange may occur on a time scale of molecular vibrations, which are at least an order of magnitude faster than rotations. It is the latter time scale of molecular rotation that reveals the participation of transient complexes via the symmetry of product angular distributions.

Figure 7 shows that both charge transfer processes yield products with internal distributions that are remarkable both in their similarities and in the fact that the distributions are independent of collision energy. The fact that the distributions show essentially no dependence on collision energy suggests that a localized, specific feature of the potential surfaces coupled by charge transfer controls the energy distributions of products. In systems in which conditions of energy resonance and favorable Franck−Condon factors play a role, this observation is readily rationalized, as in the recent studies of $D_2O^+ + C_2H_4$ and $OD^+ + C_2H_4$ charge transfer reported by our laboratory.[54,55] In those studies, the internal energy distributions directly overlapped the photoelectron spectrum of C_2H_4; their dependence on collision energy arose solely from the fact that increasing collision energy resulted in accessibility of higher internal energy Franck−Condon allowed product states. However, in the present system, the photoelectron spectrum of NH_3 shows clearly that there are no resonant states of NH_3^+ with internal energies consistent with the internal energy content of reaction products formed by charge transfer.

The experimental observations suggest that the internal energy distributions of charge transfer products are established by long distance electron transfer from NH_3 to D_2O^+, with subsequent H/D exchange processes providing only minimal modifications to the nascent distributions. However, the widths of the NH_2D^+ internal energy distributions are perceptibly larger than those of NH_3^+, suggesting that post-electron transfer interactions do play a role in the final state distribution. Additional theoretical work on the nature of the $[H_2O\cdot NH_3]^+$ system in the vicinity of nuclear configurations where electron transfer occurs is needed to understand the nature of surface couplings that establish the product internal state distributions.

The striking similarities in the flux distributions, internal energy distributions, and signal levels both for the NH_3^+ and NH_2D^+ products suggest that both kinds of collisions probe the same regions of the potential energy surface where all atoms can interact strongly with one another. Given the facile production of NH_2D^+ with a cross section comparable to NH_3^+, it is clear that motion through these regions is efficient and is much more rapid than statistically predicted. The fact that the rate for H/D exchange is 10^3 larger than predicted statistically indicates that very specific dynamical processes that are more efficient than ergodic exploration of phase space are clearly at work in this system. The results of a recent molecular dynamics simulation study[56] on the $[H_3O\cdot NH_3]^+$ system suggest a possible mechanism for nonstatistical behavior. In that study, the H_3O^+ ion is observed to first rotate into a position in which one of the H atoms is directed toward the NH_3; that is the H_3O^+ ion is

oriented by NH_3. A trajectory study[57] on the $H_3O^+ + NH_3 \rightarrow H_2O + NH_4^+$ reaction shows that the effect of the initial relative orientation of reactants is substantial, resulting in different lifetimes of intermediate complexes, and therefore different product energy distributions. Analogous orientation effects should also exist in the $[H_2O{\cdot}NH_3]^+$ system. The $[H_2O{\cdot}NH_3]^+$ complex has three probable structures, different from $[H_3O{\cdot}NH_3]^+$, which has only a linear hydrogen-bonded conformation. When D_2O^+ and NH_3 approach each other, different initial orientations of the collision partners will form different collision complexes and so lead to the production of different products. Because isomerization in complexes **1** and **2** provides pathways for H/D exchange, and these motions correspond to internal rotations, such a mechanism is worth exploring. Further dynamical studies will be essential to provide a full understanding of the above processes in this and related systems.

VII. Conclusions

The crossed molecular beam technique and density functional theory calculations have provided significant insight into the nature of the reactions between H_2O^+ (D_2O^+) and NH_3, all of which are direct, proceeding on time scales much more rapid than a rotational period of any intermediate complex. The deuterium ion transfer process to form NH_3D^+ places a significant fraction of the available energy in product vibration. Incremental translational energy appears primarily in product translation. The charge transfer processes to form NH_3^+ and NH_2D^+ have remarkably similar flux distributions, product internal energy distributions, and cross sections, despite the fact that the latter channel requires H/D exchange. This exchange process must occur on a time scale 10^3 faster than predicted by statistical theory. DFT calculations of the principal reaction pathways provide significant information about transient complexes that mediate the reactions, but additional work to understand the dynamics of charge transfer and atom exchange will be required for a complete understanding of reactions in this simple system.

Acknowledgment. We express our appreciation to the U.S. Department of Energy for financial support. We are grateful for the assistance of Li Liu and Xiaohui Cai in the experiments of this work.

Supporting Information Available: A table (Table S1) of the DFT calculated energies, vibrational frequencies, and a figure (Figure S1) of the structures are available free of charge via the Internet at http://pubs.acs.org.

References and Notes

(1) Barthel, E. R.; Martini, I. B.; Schwartz, B. J. *J. Phys. Chem. B* **2001**, *105*, 12230−12241.
(2) Rini, M.; Magnes, B.-Z.; Pines, E.; Nibbering, E. T. J. *Science* **2003**, *301*, 349−352.
(3) Meuwly, M.; Karplus, M. *J. Chem. Phys.* **2002**, *116*, 2572−2585.
(4) Sadeghi, R. R.; Cheng, H. *J. Chem. Phys.* **1999**, *111*, 2086−2094.
(5) Tomoda, S. *Faraday Discuss. Chem. Soc.* **1988**, *85*, 53−63.
(6) Tachikawa, H. *Chem. Phys.* **1996**, *211*, 305−312.
(7) Li, Y.; Liu, X.; Wang, X.; Lou, N. *Chem. Phys. Lett.* **1997**, *276*, 339−345.
(8) Ryan, P. W.; Blakley, C. R.; Vestal, M. L.; Futrell, J. H. *J. Phys. Chem.* **1980**, *84*, 561−567.
(9) Hemsworth, R. S.; Payzant, J. D.; Schiff, H. I.; Bohme, D. K. *Chem. Phys. Lett.* **1974**, *26*, 417−421.
(10) Skurski, P.; Gutowski, M. *J. Chem. Phys.* **1998**, *108*, 6303−6311.
(11) Stockman, P. A.; Bumgarner, R. E.; Suzuki, S.; Blake, G. A. *J. Chem. Phys.* **1992**, *96*, 2496−2510.
(12) Coitino, E. L.; Ventura, O. N.; Sosa, R. M. *J. Mol. Struct. (THEOCHEM)* **1992**, *254*, 315−328.
(13) Yeo, G. A.; Ford, T. A. *Can. J. Chem.* **1991**, *69*, 632−637.
(14) Lee, C.; Fitzgerald, G.; Planas, M.; Novoa, J. J. *J. Phys. Chem.* **1996**, *100*, 7398−7404.
(15) Desfrancois, C.; Baillon, B.; Schermann, J. P.; Arnold, S. T.; Hendricks, J. H.; Bowen, K. H. *Phys. Rev. Lett.* **1994**, *72*, 48−51.
(16) Shinohara, H.; Nagashima, U.; Tanaka, H.; Nishi, N. *J. Chem. Phys.* **1985**, *83*, 4183−4192.
(17) Choo, K. Y.; Shinohara, H.; Nishi, N. *Chem. Phys. Lett.* **1983**, *95*, 102−105.
(18) Kohler, G.; Janoschek, R. *J. Phys. Chem.* **1987**, *91*, 2051−2057.
(19) Reed, A. E.; Weinhold, F.; Curtiss, L. A.; Pochatko, D. J. *J. Chem. Phys.* **1986**, *84*, 5687−5705.
(20) Li, Y.; Farrar, J. M. *J. Chem. Phys.* **2004**, *120*, 199−205.
(21) *Dynamics of Molecular Collisions, Part B*; Miller, W. H., Ed.; Plenum Press: New York, 1976; Vol. 2, pp 53−120.
(22) Ding, A. M. G.; Kirsch, L. J.; Perry, D. S.; Polanyi, J. C.; Schreiber, J. L. *Faraday Discuss. Chem. Soc.* **1973**, *55*, 252−276.
(23) NIST, http://webbook.nist.gov/chemistry/om/.
(24) Anicich, V. G.; Kim, J. K.; Huntress, W. T. J. *Int. J. Mass Spectrom. Ion Phys.* **1977**, *25*, 433−438.
(25) Su, T.; Bowers, M. T. *J. Chem. Phys.* **1973**, *58*, 3027−3037.
(26) Vancura, J.; Herman, Z. *Collect. Czech. Chem. Commun.* **1988**, *53*, 2168−2174.
(27) Sodupe, M.; Oliva, A.; Bertran, J. *J. Am. Chem. Soc.* **1994**, *116*, 8249−8258.
(28) Tachibana, A.; Kawauchi, S.; Nakamura, K.; Inaba, H. *Int. J. Quantum Chem.* **1996**, *57*, 673−682.
(29) Kemper, P. R.; Bowers, M. T.; Parent, D. C.; Mauclaire, G.; Derai, R.; Marx, R. *J. Chem. Phys.* **1983**, *79*, 160−169.
(30) Chupka, W. A.; Russell, M. E. *J. Chem. Phys.* **1968**, *48*, 1527−1533.
(31) Chesnavich, W. J.; Bowers, M. T. *Chem. Phys. Lett.* **1977**, *52*, 179−183.
(32) Everest, M. A.; Poutsma, J. C.; Zare, R. N. *J. Phys. Chem. A* **1998**, *102*, 9593−9598.
(33) Green, R. J.; Zare, R. N. *J. Chem. Phys.* **1997**, *107*, 772−778.
(34) Siska, P. E. *J. Chem. Phys.* **1973**, *59*, 6052−6060.
(35) Anlauf, K. G.; Kuntz, P. J.; Maylotte, D. H.; Pacey, P. D.; Polanyi, J. C. *Discuss. Faraday Soc.* **1967**, *44*, 183.
(36) Anlauf, K. G.; Polanyi, J. C.; Wong, W. H.; Woodall, K. B. *J. Chem. Phys.* **1968**, *49*, 5189.
(37) Maylotte, D. H.; Polanyi, J. C.; Woodall, K. B. *J. Chem. Phys.* **1972**, *57*, 1547−1560.
(38) Parr, C. A.; Polanyi, J. C.; Wong, W. H. *J. Chem. Phys.* **1973**, *58*, 5.
(39) Martin, J. M. L.; Lee, T. J. *Chem. Phys. Lett.* **1996**, *258*, 129−135.
(40) Botschwina, P. *J. Chem. Soc., Faraday Trans. 2* **1988**, *84*, 1263−1276.
(41) Frisch, M. J.; Trucks, G. W.; Schlegel, H. B.; Scuseria, G. E.; Robb, M. A.; Cheeseman, J. R.; Zakrzewski, V. G.; J. A. Montgomery, J.; Stratmann, R. E.; Burant, J. C.; Dapprich, S.; Millam, J. M.; Daniels, A. D.; Kudin, K. N.; Strain, M. C.; Farkas, O.; Tomasi, J.; Barone, V.; Cossi, M.; Cammi, R.; Mennucci, B.; Pomelli, C.; Adamo, C.; Clifford, S.; Ochterski, J.; Petersson, G. A.; Ayala, P. Y.; Cui, Q.; Morokum, K.; Salvador, P.; Dannenberg, J. J.; Malick, D. K.; Rabuck, A. D.; Raghavachari, K.; Foresman, J. B.; Cioslowski, J.; Ortiz, J. V.; Baboul, A. G.; Stefanov, B. B.; Liu, G.; Liashenko, A.; Piskorz, P.; Komaromi, I.; Gomperts, R.; Martin, R. L.; Fox, D. J.; Keith, T.; Al-Laham, M. A.; Peng, C. Y.; Nanayakkara, A.; Challacombe, M.; Gill, P. M. W.; Johnson, B.; Chen, W.; Wong, M. W.; Andres, J. L.; Gonzalez, C.; Head-Gordon, M.; Replogle, E. S.; Pople, J. A. *Gaussian 98*, revision A.11.1; Gaussian, Inc.: Pittsburgh, PA, 2001.
(42) Peng, C.; Schlegel, H. B. *Isr. J. Chem.* **1994**, *33*, 449−454.
(43) Peng, C.; Ayala, P.; Schlegel, H. B.; Frisch, M. J. *J. Comput. Chem.* **1996**, *17*, 49−56.
(44) Baer, T.; Hase, W. L. *Unimolecular Reaction Dynamics: Theory and Experiments*; Oxford University Press: New York, 1996.
(45) Kassel, L. S. *J. Phys. Chem.* **1928**, *32*, 225−242.
(46) Marcus, R. A.; Rice, O. K. *J. Phys. Colloid Chem.* **1951**, *55*, 894−908.
(47) Rice, O. K.; Ramsperger, H. C. *J. Am. Chem. Soc.* **1927**, *49*, 1617−1629.
(48) Moryl, J. E.; Farrar, J. M. *J. Phys. Chem.* **1982**, *86*, 2016−2020.
(49) Moryl, J. E.; Creasy, W. R.; Farrar, J. M. *J. Chem. Phys.* **1985**, *82*, 2244−2257.
(50) Carpenter, M. A.; Zanni, M. T.; Levandier, D. J.; Varley, D. F.; Farrar, J. M. *Can. J. Chem.* **1994**, *72*, 828−835.
(51) Hirschfelder, J. O. *Int. J. Quantum Chem. Symp* **1969**, *3*, 17−31.
(52) Bueker, H.-H.; Uggerud, E. *J. Phys. Chem.* **1995**, *99*, 5945−5949.
(53) Scheiner, S.; Harding, L. B. *J. Phys. Chem.* **1983**, *87*, 1145−1153.
(54) Liu, L.; Li, Y.; Cai, X.; O'Grady, E. R.; Farrar, J. M. *J. Chem. Phys.* **2004**, *121*, 3495−3506.
(55) Cai, X.; Li, Y.; Farrar, J. M. Manuscript in preparation.
(56) Cheng, H.-P. *J. Chem. Phys.* **1996**, *105*, 6844−6855.
(57) Bueker, H.-H.; Helgaker, T.; Ruud, K.; Uggerud, E. *J. Phys. Chem.* **1996**, *100*, 15388−15392.